Photovoltaic system DC series arc fault: a case study

Alaa Hamza Omran[1], Dalila Mat Said[1], Siti Maherah Hussin[1], Sadiq H. Abdulhussain[2]

[1]Centre of Electrical Energy Systems (CEES), School of Electrical Engineering, Universiti Teknologi Malaysia (UTM), Johor, Malaysia
[2]Department of Computer Engineering, University of Baghdad, Baghdad, Iraq

Article Info

ABSTRACT

Photovoltaic (PV) systems are becoming increasingly popular; however, arc faults on the direct current (DC) side are becoming more widespread as a result of the effects of aging as well as the trend toward higher DC voltage levels, posing severe risk to human safety and system stability. The parallel arc faults present higher level of current as compared with the series arc faults, making it more difficult to spot the series arc. In this paper and For the aim of condition monitoring, the features of a DC series arc fault are Analyzed by analysing the arc features, performing model's simulation in PSCAD, and carrying out experimental studies. Various arc models are simulated and investigated; for low current arcs, the heuristic model is used where a set of parameters established. Moreover, the heuristic model's simulated arc has been shown to be compatible with the experimental data. The features of arc noise in the electrode separation region and steady-arcing states with varied gap widths are investigated. It has been discovered that after an arc fault occurs, arc noise increases, notably in the frequency range below 50 kHz; where this property is useful for detecting DC series arc faults. Besides that, variations in air gap width are more sensitive to frequencies under 5 kHz.

Corresponding Author:

Dalila Mat Said
Centre of Electrical Energy Systems (CEES), School of Electrical Engineering
Universiti Teknologi Malaysia (UTM)
81310 Johor Bahru, Johor, Malaysia
Email: dalila@utm.my

1. INTRODUCTION

Increasing the advancement of technology and the growing awareness of environmental pollution, solar energy and other clean renewable sources are gradually replacing conventional fossil fuels. Installation of solar panels is growing all over the world. The generation of grid-connected photovoltaic and rooftop solar panels will be crucial in supporting both main utility networks and micro-grids. Direct current (DC) arc problems could be caused by the increasing output of photovoltaic (PV) systems paired with the trend toward greater DC voltage levels. Improper and inadequate maintenance will sharply increase the potentiality of DC arc occurrence. Where, the long-term weathering and aging effect will deteriorate the system components such as cables, connectors and conductors [1]-[5]. It also should be mentioned that, the lack of current zero crossing in AC arcing tends to make the DC arcs more sustainable. Figure 1 depicts the PV system model with the various kinds of arc faults.

DC arcing tends to occur when connections have small gaps. Bad joints reduce the cross-sectional contact area, this will effectively increase resistance and, as a result, heat loss. The faster the connecting point deteriorates, resulting in a loose connection, the higher the operating temperature. As a result, the discontinuity

point creates a very small gap through which the current can continue to flow. When the electric field between two electrodes is larger than 3 V/μm, air begins to ionize and plasma occurs, eventually leading to the formation of a series arc. Due to the increased resistance given by the arc, the fault current will be lower than the operational current. As a result, melting the fuse or activating the overcurrent protection devices is insufficient. Unlike a parallel arc fault, a series arc fault does not produce an inverse current [3], and the normal load current will be used in contributing the total fault current. the current level decreases due to the increasing of injected impedance by the arc fault; As a result, the level required to melt the fuse cannot be reached [6]. Moreover, the level of the current will return to normal while the arcing fault remains, due to the inverter's maximum power point tracking operation; therefore, detecting DC arcing faults will be more difficult. As a result, the heat energy created by an arc may cause severe damage to system components over time, posing a serious threat to system stability and human safety [7]. For a variety of causes, parallel arcing can occur over numerous conductors or to ground, including insulation deterioration, improper wiring, effect of aging, and bites of animal [8]. Parallel arcs can be occurred between string's modules but at various string levels, as well as between the module of PV system and the ground. Because of the larger potential difference, they will draw substantially more fault current., making it simpler for conventional protection devices to detect it [9]. As a result, series arc faults which will be highlighted in this paper are frequently more challenge to be detected in PV systems than the parallel arc faults. The remainder of this work is structured as follows: In section 2, the electrical characteristics of DC series arcs are elucidated. In section 3, Various types of arc models are available. Section 4 discuss the analysis of results. Section 5 describes the experiment setup by presenting actual data. Finally, section 6 presents the conclusion.
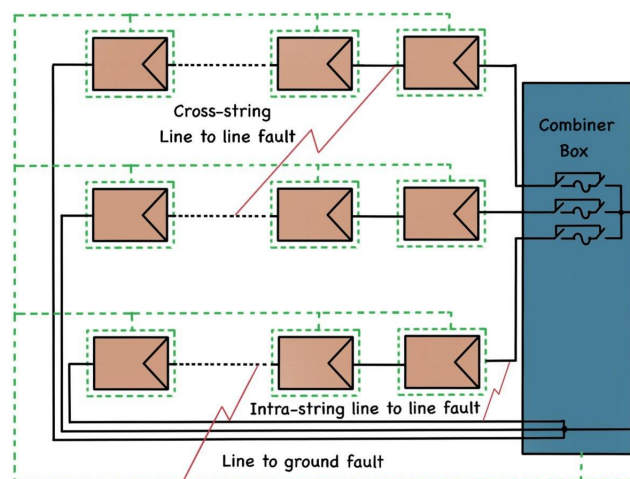

Figure 1. Different types of DC arc faults in a PV array

2. DC SERIES ARC ELECTRICAL CHARACTERISTICS

It is critical to understand and investigate the properties of an electric arcs; since it has nonlinear characteristics that vary with length of arc, material of electrode, geometry of electrode, and the level of current [10]. DC series arc can be generated between any two connecting terminals across the small gaps such as combiner box connection and the PV modules busbar-ribbon connection. The absence of scheduled maintenance, aging, affection of weather (such as rain-caused corrosion), wind that can cause the mechanical damage, bites of animal, and bad joints as a result of improper wiring. Bad joints reduce the region of the cross-section, efficaciously increasing connection resistance, and significantly increasing loss of heat. Because of the higher operating temperature, it introduces more thermal stress and accelerates connection deterioration, resulting in loose connections [11]. Following that, without interfering with current flow, a small gap will form between two connecting terminals. The air in the gap begins to ionize and the arc plasma develops, finally creating a series arc, when the electric field across the gap surpasses around 3 V/m (the breakdown strength varies depending on the surrounding environment). The flow of oxygen into the plasma stream helps to keep the discharge

of the arc going. In the case of the series arcs, the gap distance is typically in the millimetre range. In large PV systems, the level of the fault current is typically few amps at the solar cell, module, and string level, however, hundreds of amps at the combiner box can be reached and even over than a thousand of amps on the DC side of the inverter. The electrical behaviour of the arc as related to the power system can be better depicted by analysing the electrical characteristics metrics including the voltage of arc, the current of arc and the resistance of arc, and as follows:

i) Voltage of arc (V_{arc}): firstly, the arc is initiated; then, the arc voltage rises to a minimum value, that is the minimum voltage required to ignite an electric arc for the given contactor material [12], [13]. The electrode material determines the minimum arc voltage, it is unaffected by the source voltage, the current of arc, or the length of the electrode gap [14]. The arc voltage rises with a gradient as the electrode gap widens, and it is also unaffected by the DC source voltage [15]. The arc voltage remains constant when the gap length remains constant, resulting in a sustained arc.

ii) Current of arc (I_{arc}): when an arc is initiated, the arc current decreases slightly [12]. The insignificant variation that occurred due to the series arc fault will be appear in the dc circuit, on the other hand, it is difficult to be detected by the current protection units. Moreover, an increasing with a constant gradient in the arc voltage will be presented in the case of a constant resistance load, which is associated with a decreasing in the arc current. In more detail, the decreasing in the arc current will be according to a gradient that is proportional to the increasing gradient of the arc voltage [15], [13], and it will reach to a constant value simultaneously with arc voltage becomes constant.

iii) Resistance of arc (R_{arc}): because of the widespread use of the macroscopic V-I equation of arc [12], arc is considered to be resistive in general and the resistance of the arc is nonlinear. Therefore, to acquire the V-I arc characteristic, all cases of arcing conditions must be gathered, and more results of the experimental associated with the related models must be accumulated. Moreover, an inversion relationship and varies significantly depending on the arcing conditions will be exhibited. As a result, an improved understanding of arc behaviour as it relates to the electrical systems [16] will be achieved.

3. DC SERIES ARC MODELS

To recreate the DC arc as faithfully as possible, an appropriate model should be adopted. Fabian *et al.* [14] categorised models derived from physics, empirical models derived from finding the link between arc voltage and current, and heuristic models as the three primary forms of electric arc models. Nine different models of arc fault are simulated, where each model have its own several constants that allow it to simulate different cases. These models associated with their parameters are presented as follows [17]-[19]:

3.1. Ayrton model

The (1) is used to present a mathematical expression of Ayrton model. Different cases can be simulated through changing models parameters. The parameters are as follows: voltage drop of electrode (A), gradient of voltage (B), and length of arc (L). The constants C and D are the nonlinear characteristic of the arc [20].

$$V_{arc} = A + BL + \frac{C + DL}{I_{arc}} \tag{1}$$

3.2. Steinmetz model

The semi-empirical V–I equation is expressed by (2). The hard drive's composition is made up of two components: magnetite and carbon. The material of the electrodes, the form of the electrodes, and the length of the arc (L) define the constants X, Y, and Z. [21].

$$V_{arc} = A + \frac{C(Le + D)}{I_{arc}^{0.5}} \tag{2}$$

3.3. Nottingham model

To explain the phenomenon of arc, this model is based on the inverse relationship. The arc length and electrode material are inversely proportional to the constants a and b, respectively. The (3) uses the reverse current of power n, which is influenced by the electrode material and arc length. For copper electrodes with an

arc length of 1-10 mm, the power (n) is 0.67. These parameters may vary from case study to case study [22].

$$V_{arc} = A + \frac{B}{I_{arc}^n} \tag{3}$$

3.4. Hyperbolic approximation model

Equation expresses the properties of the hyperbolic approximation model (4-8). The model is represented by an analogous circuit with a variable resistor in series with the dependent voltage source and is based on a mathematical approximation (v_{gap}). Gap current (i_{gap}), Electromotive force impulse (e_{gap}), Cathode-anodic gap (x_{gap}), Variable resistance value (R_{gap}), border between quenching level and arc combustion (x_{crit}), gradient (Λ), average pre-arc DC voltage (V_{dc})) are the factors that control this model (v_q) Specific variables to control the gradient (α)[14].

$$e_{gap} = \frac{1}{2}(a + bx_{gap})(tanh(\lambda q) - tanh(\lambda(q - 1))) \tag{4}$$

$$v_q = V_{dc}\left(\frac{1}{2} + \frac{1}{2}(tanh(\alpha(q - 1)))\right) \tag{5}$$

$$v_{gap} = v_q + e_{gap} \tag{6}$$

$$q = \frac{x_{crit}}{x_{gap}} \tag{7}$$

$$R_{gap} = \frac{v_q}{i_{gap}} \approx \frac{v_{dc}}{I_{Load}}e^{2\alpha(q-1)} \tag{8}$$

3.5. Cassie model

The arc conductance of this arc model is formulated using the special equation presented by Cassie. In (9) [23], it is represented by g:

$$\frac{1}{g}\frac{dg}{dt} = \frac{1}{\tau_c}\left(\frac{v^2}{V_0^2} - 1\right) \tag{9}$$

where v denotes the arc voltage, v_0 denotes the arc length, and tau_c denotes the time constant of the conductance due to arc cross-section change, respectively. Different arc occurrence scenarios are modeled using the two parameters. The final expression of the model in (10) can be found by multiplying both sides of the equation by g.

$$\frac{1}{g}\frac{dg}{dt} = \frac{1}{\tau_c}\left(\frac{vi}{V_0^2} - g\right) \tag{10}$$

The arc voltage and current are represented by v and i respectively. Arc length and the time constant of conductance owing to arc cross-section change, respectively, are constant parameters v_0 and tau_c.

3.6. Mayr model

In his research, another major source of power dissipation during arc incidence was discovered by Mayr. To explain why, he used thermal conduction at low current values. With the use of equations, he constructed and submitted this theory (11), which shows how cross-sectional experienced significant thermal conductance. Such an effect was expressed using an equation. Mayr also assumed that the connection between voltage and current, as well as the power loss, is constant. The following equation was generated based on these considerations.

$$\frac{1}{g}\frac{dg}{dt} = \frac{1}{\tau_m}\left(\frac{P}{P_0} - 1\right) \tag{11}$$

The arc conductance, arc power, arc time constant, and cooling power are all represented by the letters g, P, τ_m, and P_0 in this equation. The final expression for the Mayr model in (12) [24] can be found by multiplying both sides of the equation by g.

$$\frac{dg}{dt} = \frac{1}{\tau_m}\left(\frac{i^2}{P_0} - g\right) \tag{12}$$

The arc conductance, arc current, and cooling power are represented by g, I and P_0, respectively. Furthermore, although Mayr's model might produce superior results for arc currents around zero, the formulas of Cassie's model could provide outstanding performance for big currents. An integration of both models and their accompanying equations will yield superior results in this regard [24], [25].

3.7. Habedank model

When the Cassie and Mayer models are connected in series, the Habedank model is created. Additional information can be found in [26]. In more detail, the overall arc conductance is described by g, u is the voltage across the arc, and i is the current flowing through arc. Furthermore, g_c and g_m are the conductance of the arcs that explained by the Cassie and Mayr equations, respectively. This model's defining parameters are the Cassie time constant (c), the Cassie constant arc voltage (U_c), and the Mayr time constant (m), which is relevant to the arc's steady state power loss (P_0).

$$\frac{dg_c}{dt} = \frac{1}{\tau_c}\left(\frac{u^2 g^2}{v_{arc}^2 g_c} - g_c\right) \tag{13}$$

$$\frac{dg_m}{dt} = \frac{1}{\tau_m}\left(\frac{u^2 g^2}{p_0} - g_m\right) \tag{14}$$

$$\frac{1}{g} = \frac{1}{g_c} + \frac{1}{g_m} \tag{15}$$

3.8. KEMA model

The KEMA arc model corresponds well to the model described by Mayer. It was created by modifying three Mayer models and connecting them in series. This model's results are very close to actual findings (more realistic results) [27].

$$\frac{dg_i}{dt} = \left(\frac{1}{\pi_i \tau_i} g_i^{\lambda_i} u_i^2 - \frac{1}{\tau_i} g_i\right) \tag{16}$$

$$\frac{1}{g} = \sum_{i=1}^{a} \frac{1}{g_i} \tag{17}$$

$$u = \sum_{i=1}^{3} u_i \tag{18}$$

$$i = gu \tag{19}$$

3.9. Schwarz model

Mayer's arc model is modified in some way that the cooling power and time constant are affected by arc conductance. Schwarz created this modulation, and the model bears his name. Additional details can be found in [28]. A number of adjustable parameters was used to describe this model such as arc time constant (τ), cooling constant (P), and two other parameters, namely, τ_a and P_b, that impact the dependency of conductance.

$$\frac{1}{g}\frac{dg}{dt} = \frac{d\ln g}{dt} = \frac{1}{\tau g^a}\left(\frac{ui}{Pg^b} - 1\right) \tag{20}$$

Finally, the models presented are used to create a massive dataset. PSCAD software is used to analyze these models, and the effects of the parameters are investigated and presented in a variety of scenarios.

4. RESULTS ANALYSIS AND DISCUSSION

PSCAD software creates and simulate various arc fault models. Nine arc approaches section 3 are used to produce the required records by varying factors such as arc length, irradiance, Switching frequency of the inverter, load current, and temperature These parameters were employed to improve results, and a huge number of records were created that were expected to cover all of the predicted fault instances that the PV system could face. Furthermore, the records produced can be classified as follows:

i) A database of records devoted to the inverter's initialization.

ii) A database of records devoted to changing the load setup.

iii) A collection of records devoted to series arc fault.

iv) A database of records devoted to series arc faults.

v) Further cases of arc problems collection of records.

With 6,000 data points, the total number of records generated was roughly 800. The records are normalized based on the length of the window. To develop the detection method, data is trained using the specified schema after sample normalization.

4.1. Changes in inverter start-up and load setup records

This set of data was derived from the created records in order to show two major scenarios that can be regarded typical PV system behavior. The first is the startup of the inverter. The load change is the second normal behavior of the PV system. Variability in the PV system's output voltage is caused by inverter start-up and/or load shift, which changes according to these circumstances. Several instances of inverter startup and load change are shown in Figure 2, where the inverter startup and load change are depict in Figures 2(a) and 2(b), respectively.
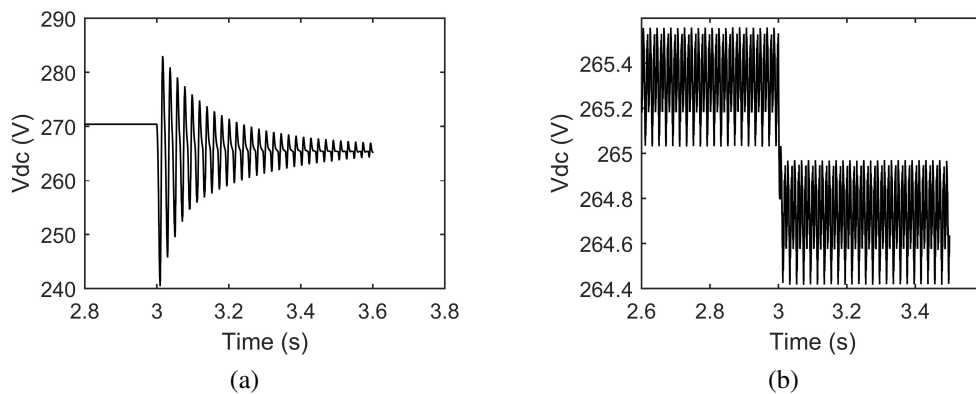
Figure 2. Normal case sample: (a) inverter start-up and (b) load changes

4.2. Other faults cases records

Figure 3 shown the data which are linked to other failures that can occur in a PV system are short circuit fault and capacitor switching as illustrated in Figure 3(a), Figure 3(b), and Figure 3(c), respectively. All such records are created to improve the detection method's performance by distinguishing between various disturbances and the series arc.
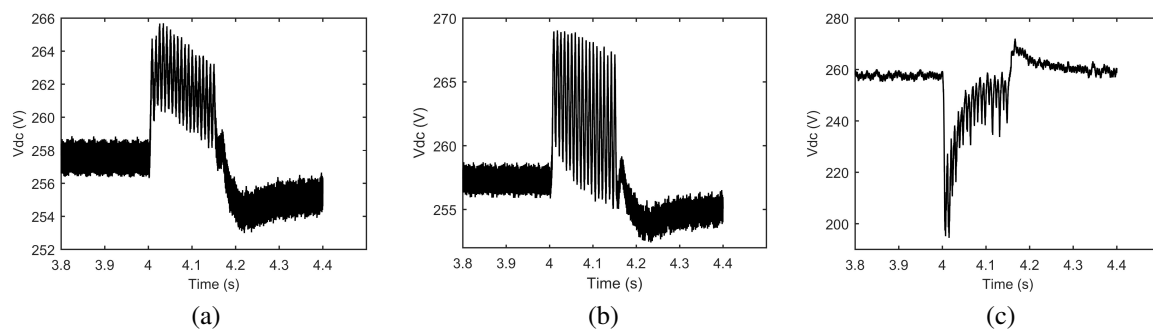

Figure 3. Different samples of faults: (a)short circuit, (b) short circuit, and (c) capacitor circuit

4.3. Series arc fault records

These records demonstrates the series arc fault, Figure 4 shown different nine models of DC series arc fault are used which are Ayrton, Cassie, Habedank, Hyperbolic, Kema, Nottingham, Schwarz, Steinmetz and Mayer as shown in Figure 4(a), Figure 4(b), Figure 4(c), Figure 4(d), Figure 4(e), Figure 4(f), Figure 4(g), Figure 4(h), and Figure 4(i), respectively. Nevertheless, in actuality, several aspects such as improper installation, infrequent maintenance, and environmental impacts cause this kind of fault to arise. The proposed approach was trained to identify it precisely. More specifically, the Ayrton model also includes the only minimum concentration of current that relates to the V-I characteristic group. The cassie model, on the other hand, belongs to the physical-based group, which tends to work with a high level of current and is dependent on the gap between the two electrodes. Furthermore, the two other models, Habedank and Hyperbolic, contain both current, low, and high levels. Nevertheless, they are similar to the cassie model in that they are dependent on the gap between the two electrodes; however, they belong to a various group of arc model-based models. The Habdenk arc model is physics-based, whereas the hyperbolic arc model is heuristic. The other models, Schwarz, Steinmetz, and Mayer, enclosed the low level of current and are similar to the earlier mentioned models that rely on the electrode gap. Schwarz and Mayer are physics-based, whereas Steinmetz is V-I characteristic-based. Table 1 [29] provides a summary of these arc fault models.
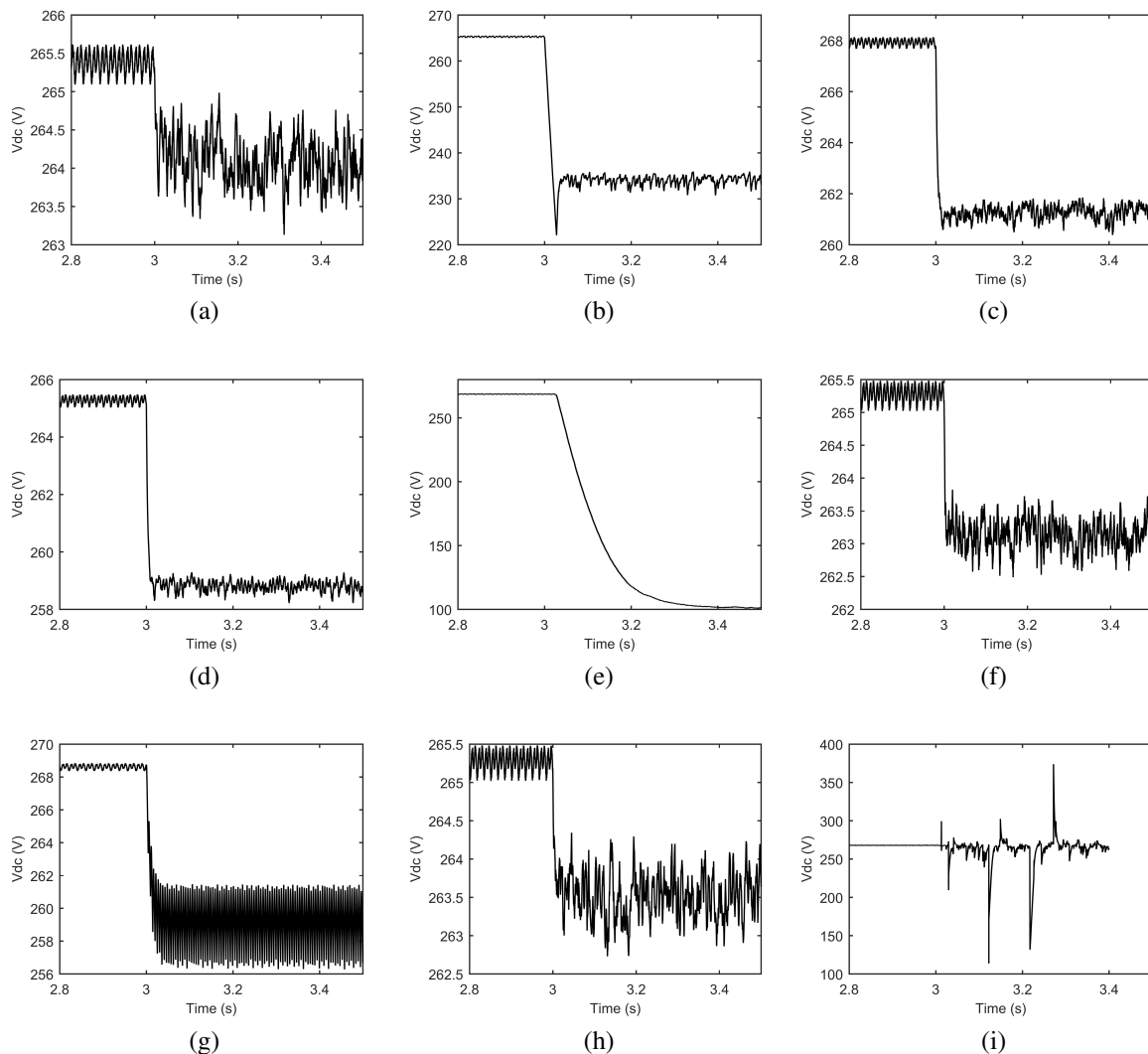

Figure 4. Series arc fault signals of different models (a) Ayrton, (b) Cassie, (c) Habedank, (d) Hyperbolic, (e) Kema, (f) Nottingham, (g) Schwarz, (h) Steinmetz, and (i) Mayer

Table 1. Arc fault models summary

Arc model	Current level	Two electrodes gap width (mm)	Series arc fault	Model type
Ayrton	Low	1–10 mm	Yes, at below string level	V-I characteristic-based arc model
Cassie	High	Depends	Yes, at the array level	Physics-based arc model
Habedank	Low/High	Depends	Yes	Physics-based arc model
Hyperbolic	Low/High	Depends	Yes	Heuristic arc
Kema	High	Depends	Yes	Physics-based arc model
Nottingham	Low (below 10 A)	1–10 mm	Yes, at below string level	V-I characteristic-based arc model
Schwarz	Low	Depends	Yes, at below string level	Physics-based arc model
Steinmetz	Low	Depends	Yes, at below string level	V-I characteristic-based arc model
Mayer	Low	Depends	Yes, at below string level	Physics-based arc model

5. EXPERIMENTAL SETUP

The experiment is intended to determine the impact of changing values of the DC supply voltage, load current, input load capacitance, and cable inductance on the characteristics of DC series arc. The experimental results would be illustrated to demonstrate the various DC series arc responses according to different conditions of circuit parameters, providing more information for determining the triggering value of the DC series arc detection method. The experimental set-up was utilized to validate the simulation model results by describing the arc characteristics. The load side capacitor voltage measurement data was passed through the devised algorithm after arcs were formed on the experimental setup. This section conducts off-line investigations for arcing experiments with noisy power supplies; the experimental setup equivalent circuit can be shown in Figure 5. The experimental parameters used to define the behaviour of DC series arc fault are listed in Table 2.
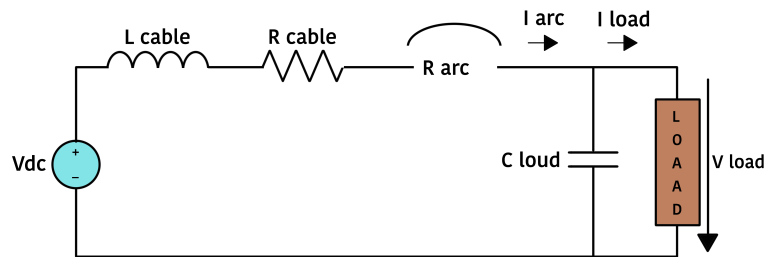

Figure 5. Experimental setup equivalent circuit

Table 2. Parameters of arc behaviour experimental

Parameters	Symbol	Values
DC voltage	V_{dc}	$48V, 75V, 100V$
Load current	I_{Load}	$3A, 4A, 5A$

In the Electrical Engineering Department, College of Engineering, University of Technology, Baghdad, Iraq, a series of experiments were carried out. The experimental setup regarding to the equivalent circuit depicts in Figure 6. However, the measured data on load capacitor voltage during an arcing scenario associated with a noisy supply which formed the typical computation is depicted in Figure 7.

In this experiment, a series arc ignites for approximately eight seconds for width of 3 mm across air gap (where adjusting the gap distance took three seconds while burning the arc in steadily case took five second); subsequently, the arc extinguished by turning off the power source. The lower the frequency resolution, the smaller window size, and the more inaccurate the spectrum information results. A larger window size, on the other hand, provide high frequencies resolution at the expense of a longer period of time delay. As a result, a window size of 0.2 s provides a good mix of precision and delay. As a consequence:

i) During the initial ignition stage of an arc fault, all frequency components magnitude increases, especially in the lower 50 kHz frequency band. It's crucial for the creation of an arc fault detecting technique.

ii) After the arc is ignited, the arc noise intensity will be less, however, it will still be greater than in the non-arcing stage.

iii) With increasing arc gap width during different steady arcing states, the frequency contents magnitude that lower than 5 kHz increases, however, it remains roughly constant outside of this range.

iv) As can be seen, the arc noise floor rises during the separation process. Furthermore, contents with a lower frequency, such as 5 kHz, are far more sensitive to variations in air gap width.
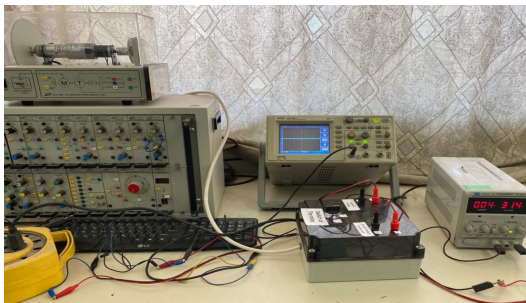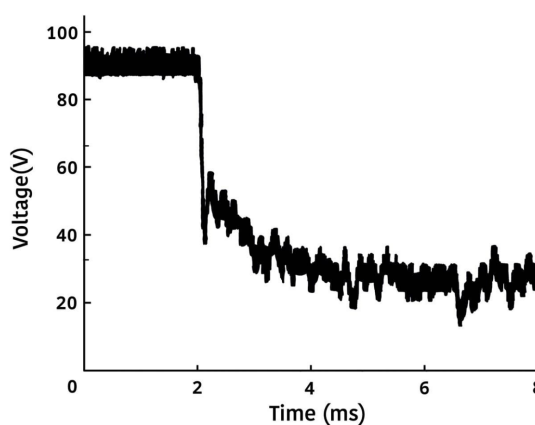

Figure 6. Experimental setup

Figure 7. DC Series arc signal as an experimental results

6.   CONCLUSION

For DC series arc faults, the arc fault characteristics of arc voltages, arc current, and arc resistance have been experimentally measured. However, in order to analyze the series arc characteristics of the DC power distribution system, PSCAD software is utilized to simulate nine different arc models. With 6,000 data points, the total number of records generated was roughly 800. The records are normalized based on the length of the window. Furthermore, a large number of experimental tests were performed in which arcs signals were generated in the experimental setup and measurement data for the load side capacitor voltage was collected. More specifically, the experiment was designed to validate the simulated arc signals based on the various arcs models. Arc experiments can be used to extract and validate the arc model. As a result, the arc models are ready for use as a simulation tool in the development of arc fault detection methods for complicated power systems at the DC side.

REFERENCES

[1]   J. Lee and G.-L. Park, "Renewable energy allocation based on maximum flow modelling within a microgrid," *International Journal of Electrical and Computer Engineering (IJECE)*, vol. 12, no. 2, pp. 1180–1188, Apr. 2022, doi: 10.11591/ijece.v12i2.pp1180-1188.
[2]   R. Malemnganbi and B. A. Shimray, "An integrated multiple layer perceptron-genetic algorithm decision support system for photovoltaic power plant site selection," *International Journal of Electrical and Computer Engineering (IJECE)*, vol. 12, no. 2, pp. 1965–1972, Apr. 2022, doi: 10.11591/ijece.v12i2.pp1965-1972.
[3]   V. M. Levin and A. A. Yahya, "An innovative method of fault detection in power transformers," *International Journal of Electrical and Computer Engineering (IJECE)*, vol. 12, no. 2, pp. 1123–1130, Apr. 2022, doi: 10.11591/ijece.v12i2.pp1123-1130.
[4]   A. H. Omran, D. Mat Said, S. H. Abdulhussain, S. M. Hussin, and N. Ahmad, "Models, detection methods, and challenges in DC arc fault: a review," *Jurnal Teknologi, vol. 83, no. 4, pp. 1–16, Jun. 2021, doi: 10.11113/jurnalteknologi.v83.15101.*
[5]   A. H. Omran, D. M. Said, S. M. Hussin, S. H. Abdulhussain, and N. Ahmad, "A survey of different DC faults in a solar power system," in *2020 IEEE 8th Conference on Systems, Process and Control (ICSPC)*, Dec. 2020, pp. 13–18, doi: 10.1109/ICSPC50992.2020.9305810.
[6]   C. Strobl and P. Meckler, "Arc faults in photovoltaic systems," *2010 Proceedings of the 56th IEEE Holm Conference on Electrical Contacts*, 2010, pp. 1-7, doi: 10.1109/HOLM.2010.5619538.
[7]   M. W. Earley and J. S. Sargent, *National Electrical Code 2011 Handbook*, 12th ed. Quincy, MA, USA: National Fire Protection Association, 2010, pp. 181–193.
[8]   Z. Wang, S. McConnell, R. S. Balog, and J. Johnson, "Arc fault signal detection - Fourier transformation vs. wavelet decomposition techniques using synthesized data," *2014 IEEE 40th Photovoltaic Specialist Conference (PVSC)*, 2014, pp. 3239-3244, doi: 10.1109/PVSC.2014.6925625.
[9]   Z. Wang and R. S. Balog, "Arc fault and flash signal analysis in DC distribution systems using wavelet transformation," *IEEE Transactions on Smart Grid*, vol. 6, no. 4, pp. 1955-1963, July 2015, doi: 10.1109/TSG.2015.2407868.
[10]   J. Yuventi, "DC electric arc-flash hazard-risk evaluation for photovoltaic systems," *EEE Transactions on Power Delivery*, vol. 29, no. 1, pp. 161-167, Feb. 2014, doi: 10.1109/TPWRD.2013.2289921.
[11]   R. F. Ammerman, T. Gammon, P. K. Sen, and J. P. Nelson, "DC-Arc models and incident-energy calculations," *IEEE Transactions on Industry Applications*, vol. 46, no. 5, pp. 1810-1819, Sept.-Oct. 2010, doi: 10.1109/TIA.2010.2057497.
[12]   F. Reil, A. Sepanski, W. Herrmann, J. Althaus, W. Vaaßen, and H. Schmidt, "Qualification of arcing risks in PV modules," *2012 38th IEEE Photovoltaic Specialists Conference*, 2012, pp. 000727-000730, doi: 10.1109/PVSC.2012.6317709.
[13]   J. D. Park and J. Candelaria, "Fault detection and isolation in low-voltage dc-bus microgrid system," *IEEE Transactions on Power Delivery*, vol. 28, no. 2, pp. 779-787, April 2013, doi: 10.1109/TPWRD.2013.2243478.
[14]   F. M. Uriarte *et al.*, "A DC arc model for series faults in low voltage microgrids," *IEEE Transactions on Smart Grid*, vol. 3, no. 4, pp. 2063-2070, Dec. 2012, doi: 10.1109/TSG.2012.2201757.
[15]   J. Li, D. W. P. Thomas, M. Sumner, E. Christopher, and Y. Cao, "Series arc fault studies and modeling for a DC distribution system," *2013 IEEE PES Asia-Pacific Power and Energy Engineering Conference (APPEEC), 2013, pp. 1-6, doi: 10.1109/APPEEC.2013.6837250.*
[16]   X. Yao, L. Herrera, and J. Wang, "Impact evaluation of series DC arc faults in DC microgrids," *2015 IEEE Applied Power Electronics Conference and Exposition (APEC)*, 2015, pp. 2953-2958, doi: 10.1109/APEC.2015.7104771.
[17]   K. J. Tseng and G. Luo, "Power electronic-based protection for direct-current power distribution in micro-grids," *2014 International Power Electronics Conference (IPEC-Hiroshima 2014 - ECCE ASIA)*, 2014, pp. 2145-2151, doi: 10.1109/IPEC.2014.6869885.
[18]   A. H. Omran, D. M. Said, S. M. Hussin, S. H. Abdulhussain, N. Ahmad, and H. Samet, "A novel intelligent detection schema of series arc fault in photovoltaic (PV) system based convolutional neural network," *Periodicals of Engineering and Natural Sciences*, vol. 8, no. 3, pp. 1641–1653, 2020, doi: 10.21533/pen.v8i3.1566.
[19]   A. H. Omran, D. M. Said, S. M. Hussin, S. M Mirsaeidi, and Y. M. Abid, "An intelligent classification method of series arc fault models using deep learning algorithm," *2020 IEEE International Conference on Power and Energy (PECon)*, 2020, pp. 44-48, doi: 10.1109/PECon48942.2020.9314520.
[20]   H. Ayrton, *The electric arc*, Cambridge University Press, 2012.
[21]   C. P. Steinmetz, "Electric power into light, Section VI. The arc," *Transactions of American Institute of Electrical Engineers*, vol. 25, p. 802, 1906.
[22]   T. Gammon, W.-J. Lee, Z. Zhang, and B. C. Johnson, "A review of commonly used DC arc models," *Conference Record of 2014 Annual Pulp and Paper Industry Technical Conference*, 2014, pp. 34–43, doi: 10.1109/PPIC.2014.6871146.
[23]   A. M. Cassie, "Theorie Nouvelle des Arcs de Rupture et de la Rigidité des Circuits," *Cigre*, vol. 102, pp. 588–608, 1939.
[24]   O. Mayr, "Beiträge zur Theorie des statischen und des dynamischen Lichtbogens," *Archiv für Elektrotechnik*, vol. 37, no. 12, pp. 588–608, Dec. 1943, doi: 10.1007/BF02084317.
[25]   O. Mayr, "Über die Theorie des Lichtbogens und seiner Löschung," *Archiv für Elektrotechnik*, vol. 44, no. 4, pp. 203–233, Apr. 1959, doi: 10.1007/BF01574721.
[26]   U. Habedank, "On the mathematical description of arc behaviour in the vicinity of current zero," *etzArchiv*, vol. 10, pp. 339–343, 1988.
[27]   R. P. P. Smeets and V. Kertesz, "Evaluation of high-voltage circuit breaker performance with a new validated arc model," *IEE Proceedings - Generation, Transmission and Distribution*, vol. 147, no. 2, p. 121, 2000, doi: 10.1049/ip-gtd:20000238.
[28]   J. Schwarz, "Dynamisches verhalten eines gasbeblasenen turbulenzbestimmten schaltlichtbogens," *ETZ-A*, vol. 92, no. 3, pp. 389–391, 1971.
[29]   S. Lu , B. T. Phung, and D. Zhang , "A comprehensive review on DC arc faults and their diagnosis methods in photovoltaic systems," *Renewable and Sustainable Energy Reviews*, vol. 89, pp. 88–98, Jun. 2018, doi: 10.1016/j.rser.2018.03.010.

BIOGRAPHIES OF AUTHORS

Alaa Hamza Omran received her M.Sc. in computer engineering from baghdad university, Iraq. She is a PhD. Student at Universiti Teknologi Malaysia, Malysia since 2019. Here main research is application of intelligent system in power system protection and operation. She can be contacted at email: alaa.hamza90@uoitc.edu.iq.

Dalila Mat Said is a Senior Lecturer at Centre of Electrical Energy Systems, School of Electrical Engineering, Universiti Teknologi Malaysia, Johor, Malaysia. She received the B.Eng. in M.Eng and PhD degrees in electrical engineering from Universiti Teknologi Malaysia in 2000, 2003 and 2012 respectively. She has experience within the area of power quality consultancy. She was involved in the Power Quality Baseline Study in Peninsular Malaysia (2010–2013) under the Energy Commission of Malaysia. She is a senior member of Institute Electrical Electronic Engineer (SMIEEE), Registered Graduate Engineer with the Board of Engineers Malaysia (BEM), Graduate Member of Institution of Engineers Malaysia (IEM) and Professional Technologist of Malaysia Board of Technologies. Her research interests are power quality and power system measurement and monitoring. She can be contacted at email: dalila@utm.my.

Siti Maherah bt Hussin is a Senior Lecturer at School of Electrical Engineering, Faculty of Engineering, Universiti Teknologi Malaysia (UTM), Johor Bahru. She received her Bachelor of Electrical Engineering in 2009 with first class honours, Master of Engineering (Electrical-Power) in 2011 and PhD in Coordinated Generation and Transmission Maintenance Scheduling Using Mixed Integer Linear Programming from Universiti Teknologi Malaysia. Her research interest is in Power System Planning, and Renewable Energy. She can be contacted at email: sitimaherah@utm.my.

Sadiq H. Abdulhussain was born in Baghdad, Iraq, in 1976. He received the B.Sc. and M.Sc. degrees in electrical engineering from Baghdad University, in 1998 and 2001, respectively. Received the Ph.D. degree from Universiti Putra Malaysiain 2018. Since 2005, he has been a staff member with the Computer Engineering Department, Faculty of Engineering, University of Baghdad. His research interests include computer vision, signal processing, as well as speech and image processing. He can be contacted at email: sadiqhabeeb@coeng.uobaghdad.edu.iq.